Range expansion to record-breaking elevations influences, but does not eliminate, *Batrachochytrium dendrobatidis* infections for Andean anurans

Emma Steigerwald[1, 2], Cassandra Gendron[3], Juan C. Chaparro[4], Rosemary G. Gillespie[2], Allie Byrne[1, 2], Rasmus Nielsen[5, 6, 7], Bree Rosenblum[1, 2]

[1] The Museum of Vertebrate Zoology, The University of California at Berkeley, CA, 94720, USA
[2] The Department of Environmental Science, Policy, and Management, The University of California at Berkeley, CA, 94720, USA
[3] The Department of Plant and Microbial Biology, The University of California at Berkeley, CA, 94720, USA America
[4] El Museo de Biodiversidad del Perú, Cusco, Perú
[5] The Department of Integrative Biology, The University of California at Berkeley at Berkeley, CA, 94720, USA
[6] The Department of Statistics, The University of California at Berkeley at Berkeley, CA, 94720, USA
[7] The Globe Institute, The University of Copenhagen, 1350, København K, Denmark

ABSTRACT

Climate change impacts emerging infectious disease events through multiple mechanisms, but the influence it exerts through driving host range shifts has been little explored. For instance, range shifts may affect pathogen transmission by altering the connectivity of host populations.

Additionally, range expanding hosts and pathogens will have different physiological responses to the suites of novel, challenging conditions they are exposed to, influencing infection outcomes. We studied the fungal pathogen *Batrachochytrium dendrobatidis* (*Bd*) on three amphibians in the Cordillera Vilcanota, Peru: *Pleurodema marmoratum*, *Telmatobius marmoratus*, and *Rhinella spinulosa*. There, these species have undergone a climate-driven range expansion into recently deglaciated habitat to become both the highest elevation amphibians and the highest elevation cases of *Bd* infection globally. We analyzed *Bd* genetics, infection metrics, and apparent sublethal impacts along the colonization front (3,900—5,400 m asl) to explore how elevational range expansion affected host-pathogen dynamics. Amphibian range shifts have enabled new connectivity across the once continuously glaciated Cordillera Vilcanota, but genetic evidence suggests that *Bd* disperses so frequently and extensively that this novel connectivity has not contributed significantly to overall *Bd* dispersal. Although amphibians have not escaped *Bd* infection outright through upslope expansion in the Cordillera Vilcanota, *Bd* growth does appear to be constrained at the highest reaches of the Vilcanota. We present evidence that *Bd* infection has different sublethal costs for amphibians at the new elevations they have colonized, though whether the costs are mitigated or exacerbated by extreme elevation may be moderated by amphibian microhabitat use.

KEYWORDS:

Batrachochytrium dendrobatidis — climate change— disease triangle — elevational gradient — range expansion—sublethal effects —synergisms — transmission

INTRODUCTION

The rising incidence of emerging infectious diseases (EIDs) is a critical issue for both conservation and public health (Jones *et al.* 2008, Fisher *et al.* 2012). Climate change may be contributing to increased outbreaks by providing pathogens with opportunities to switch hosts, expand geographically, or become more virulent (Harvell *et al.* 2002, Hoberg and Brooks 2015, Liang and Gong 2017). One little-studied mechanism by which climate change might influence the course of EIDs is by driving hosts to shift their geographic ranges (Parmesan *et al.* 1999, Moritz *et al.* 2008, Freeman *et al.* 2018). As hosts undergo range shifts, their exposure to novel environments may alter host-pathogen dynamics—potentially exacerbating or mitigating infections, affecting transmission patterns, or exposing hosts to new pathogens.

Climate-driven range shifts are expected to influence the infection dynamics of several important pathogens, with profound implications for the wellbeing of humans and biodiversity. In Hawaii, the upslope range shifts of mosquitos are predicted to drive the continuing decline of endemic birds currently finding refuge from avian malaria at high elevations (Zamora-Vilchis et al 2012), and in Europe the northwards expansion of ticks is predicted to increase the spatial extent of Lymes infections (Jaenson and Lindgren 2011). Most of the data we currently have on the interaction of climate-driven range shifts and EIDs comes from vector-borne pathogen systems, as the biology of many vectors is highly sensitive to climate (Harvell et al 2002). Although this interaction is also relevant to pathogens that rely direct transmission between hosts, these situations are so far little documented.

The emergence of *Batrachochytrium dendrobatidis* (*Bd*), the pathogen causing chytridiomycosis that has contributed to devastating global amphibian declines (Skerratt *et al.* 2007, Scheele *et al.* 2019), has been linked to climate change through a few proposed mechanisms (Li *et al.* 2013). Climate change could expand the spatial extent of optimal *Bd* growth conditions (Bosch *et al.* 2007). Meanwhile, more frequent droughts compromise amphibian immunity and enhances *Bd* transmission through amphibian aggregation in wet or humid microhabitats (Burrowes *et al.* 2004, Lampo *et al.* 2006). Higher climatic variability may also favor rapidly-adapting pathogens over hosts, resulting in worse infections (Rohr and Raffel 2010, Raffel *et al.* 2013). Finally, as parasites generally have broader thermal tolerances than hosts, frogs are likely to be exposed to suboptimal temperatures before *Bd*, placing them at a disadvantage (Cohen *et al.* 2017, 2019). The mounting evidence that amphibians are range shifting across the world (e.g. Bustamante *et al.* 2005, Raxworthy *et al.* 2008, Enriquez-Urzelai *et al.* 2019) suggests another link between climate change and amphibian-*Bd* dynamics: colonization and exposure to novel environments.

The Cordillera Vilcanota, in southern Peru, presents an ideal system for exploring how climate-driven range shifts impact EIDs. Field surveys of this heavily glaciated tropical mountain chain in the early 2000s documented the first known *Bd* infections in southern Peru (Seimon *et al.* 2005), but also revealed that three frog species had expanded their elevational ranges by hundreds of vertical meters into mountain passes that were fully glaciated at the end of the Little Ice Age, only 150 years ago. The Marbled four-eyed frog (*Pleurodema marmoratum*) had expanded upslope to 5,400 m asl, making it the highest elevation amphibian in the world; the Andean toad (*Rhinella spinulosa*) and Marbled water frog (*Telmatobius marmoratus*) had expanded to 5,244 m asl (Seimon *et al.* 2007). Chytridiomycosis was recorded in *P. marmoratum*

98 and *T. marmoratus* at the upper limits of their distribution, and a die-off event was observed in *T.*
99 *marmoratus* at 5,244 m asl (Seimon *et al.* 2007). Today, all three frogs persist in the Vilcanota,
100 though at lower abundances, and host-pathogen dynamics have transitioned into a more stable,
101 enzootic state (Seimon et al 2017), as can also be said of neighboring frog communities
102 downslope (Catenazzi *et al.* 2017).
103
104 Moving upslope in the Vilcanota, *Bd* and frogs are challenged by increasingly inhospitable
105 conditions: progressively more intense UV radiation, deep frozen precipitation, and a partial
106 oxygen pressure 50-60% of that at sea level (Wang *et al.* 2014, Poremba *et al.* 2015, Seimon *et*
107 *al.* 2017). At the apex of the Vilcanota mountain passes, soil temperature can dip to –12°C at
108 night and reach 25°C during the day, with a soil freezing rate exceeding that measured from any
109 site on Earth (1.8°C h^{-1} ; Schmidt *et al.* 2009). Resident frogs can be exposed to an even broader
110 operative temperature range (−3.5 to 44°C; Reider 2018). Here, we asked how range expansion
111 into these new, challenging elevations may have influenced *Bd* infection dynamics. We used
112 genetic data to inform our understanding of the local history of *Bd*, then examined site-level
113 infection metrics and apparent sublethal infection impacts to understand how conditions at
114 newly-colonized elevations might sway infection outcomes. We anticipate that *Bd* in the
115 Vilcanota is from the global panzootic lineage (*Bd*GPL), the lineage largely responsible for *Bd*
116 epizootics in South America (James *et al.* 2015), though these highest elevations inhabited by *Bd*
117 presumably impose strong selective pressures that could conceivably result in a limited number
118 of locally-adapted *Bd*GPL strains proliferating. If *Bd* remains dispersive despite extreme high-
119 elevation conditions, and particularly if it was introduced to the Vilcanota just before die-offs
120 occurred there in the early 2000s, *Bd* will be spatially unstructured, a common finding elsewhere

Bd population genetics have been studied (e.g. Byrne *et al.* 2019, Alvarado-Rybak *et al.* 2021, Basanta *et al.* 2021). However, if the environmental persistence of *Bd* is depressed by harsh, high elevation conditions, the genetic structure of *Bd* is more likely to reflect its gradual spread between watersheds by way of frog dispersal along the corridors provided by deglaciated mountain passes (Haddad *et al.* 2014). The present study is the first to examine *Bd* infection dynamics above 4000m asl (3,900—5,400 m asl); though *Bd* infection prevalence and intensity tend to initially increase with elevation, studies sampling to 4000 m asl suggest that these metrics may begin to decline again with increasing elevations (Muths *et al.* 2008, Catenazzi *et al.* 2011). For this reason, we expect *Bd* infection to have lower sublethal impacts for amphibians at newly-colonized, extreme high elevation sites. Alternatively, if the stress of high elevations and *Bd* infection impact amphibians synergistically, the sublethal impacts of *Bd* may increase with elevation. These analyses provide the first insights into how the contemporary, climate-driven range shifts of hosts may influence EID events.

MATERIALS AND METHODS

Fieldwork

The Cordillera Vilcanota (13.74˚S, 71.09˚W) is an 80 km-long mountain chain in the southern Peruvian Andes, crossing the departments of Cusco and Puno. We sampled *P. marmoratum*, *R. spinulosa,* and *T. marmoratus* during the transition between the wet and dry seasons (March-May) in 2018 and 2019. Whereas *T. marmoratus* breed throughout the year, *P. marmoratum* and *R. spinulosa* are in their final months of reproductive activity at this time, such that tadpoles can

143 be sampled even when adults are difficult to locate. We sampled at 76 sites across three
144 watersheds: the Alto Urubamba on the interandean versant and the Inambari and Yavero on the
145 Amazonian versant. Sites ranged from 3,967—5,333 m asl, including transects across two
146 deglaciated passes (Fig. 1). We spent approximately equal person-hours at each sampling site,
147 capturing tadpoles by scoop net and searching for post-metamorphic stages under rocks and
148 along the edges of water bodies. We attempted to capture 15 adults per species per site. If we
149 could not locate 15 adults, we supplemented first with juveniles and then with tadpoles. We
150 sampled 695 *P. marmoratum* (317 adults), 173 *Rhinella spinulosa* (82 adults), and 232 *T.*
151 *marmoratus* (23 adults).
152
153 Post-metamorphic individuals were dry swabbed 7X along the ventral surface of each limb and
154 the vascular patch to assess *Bd* infection; tadpole mouthparts were swabbed 25X (MW113,
155 Medical Wire & Equipment Co., Ltd., Corsham, Wiltshire, UK; Boyle *et al.* 2007). Swabs were
156 air dried and stored dry or in 80% ethanol. We collected 30 paired dry- and ethanol-stored swabs
157 to compare their efficacy in preserving *Bd* DNA. We noted snout-vent length (SVL), mass, sex,
158 and signs of disease in adults (lethargy, excessive sloughing, reddened skin). Individuals with
159 nuptial pads were considered adult males. Adult male SVL were used to derive a lower-end size
160 threshold for classifying adults, since males of these species are smaller than females: 19mm for
161 *P. marmoratum*; 30mm for *R. spinulosa*; and 29mm for *T. marmoratus*. Post-metamorphic
162 individuals without nuptial pads that exceeded this threshold were classed as adult females. We
163 also recorded SVL, mass, and signs of disease in juveniles; as well as SVL, mass, and Gosner
164 developmental stage (Gosner 1960) in tadpoles. Samples were transported to the University of
165 California, Berkeley for -80˚C storage.

DS1921G Thermocron Temperature Loggers (OnSolution Pty Ltd, Sydney, Australia; hereafter, 'iButtons') were placed at a subset of 20 sampling sites during the 2018 sampling season, with paired iButtons deployed to measure temperature every four hours in aquatic and terrestrial microhabitats. Aquatic iButtons were protected with rubber spray sealant, glued to the inside of a 3cm-diameter PVC tube of 12cm length, and placed in ephemeral ponds containing *P. marmoratum* tadpoles. Terrestrial iButtons were glued to the inside of a 10cm funnel, which was placed upside down and covered with rocks in location where adult *P. marmoratum* occurred. Data was downloaded from recovered iButtons during the 2019 sampling season.

Bd quantification and genotyping

We focused on gaining a comprehensive understanding of Bd dynamics in our most widely-sampled frog, *P. marmoratum.* We estimated *Bd* zoospore equivalents (ZE) per swab using triplicate quantitative PCR reactions (Hyatt *et al.* 2007). There was no difference between ethanol and dry-stored *Bd* swabs (see Supporting information for details). Amplicon sequencing libraries were prepared for 96 *Bd*+ extracts, selected to maximize the geographic representation of sampling, on a Fluidigm Access Array and sequenced with Illumina Miseq (Byrne *et al.* 2017). We processed sequences with the reduce_amplicons.R script (https://github.com/msettles/dbcAmplicons) and produced BAM files and ambiguity sequences as substrates for the following analyses (see Supporting Information for details).

Phylogenetic, structure, and redundancy analyses

Importing ambiguity sequences for Vilcanota samples and previously published sequence data representative of global *Bd* diversity (Byrne *et al.* 2019) into R, we removed one sample for each of six amplicons that resulted in >5bp length differences, samples with >80% missing amplicons, and amplicons with >33.3% missing samples. We aligned filtered ambiguity sequences in MUSCLE (v3.32; Edgar 2004). In Geneious (v2021.1.1), we checked for alignment issues and estimated a ML gene tree for each amplicon using RAxML (v4.0) with the GTR substitution model and the rapid bootstrapping method for 100 bootstraps. We collapsed gene trees in Newick Utils (v. 1.6) by branches with <10 bootstrap support to improve tree accuracy, then estimated an unrooted species tree in ASTRAL (v5.7.4) and visualized in GGTREE (v3.0.2).

To examine standing genetic variation of Vilcanota *Bd*, we used BAM files to create a Site Frequency Spectrum (SFS) in ANGSD (v0.933-106-gb0d8011). BAMs were then processed separately for the subset of Vilcanota samples retained in phylogenetic analyses and the larger dataset including globally representative *Bd*GPL samples (Byrne *et al.* 2019). We indexed BAMs in SAMtools (v1.11) and detected variants with a minimum coverage of 10X in FreeBayes (v1.3.2-46-g2c1e395). We conducted a principal component analysis with a NIPALS PCA based on an ANGSD covariance matrix (Korneliussen *et al.* 2014), a method only evaluating pairwise sets of individuals at loci for which they are both sequenced. We tested for population structure at the scale of sampling sites and watersheds, using a pegas-based, clone-corrected AMOVA in Poppr (Kamvar *et al.* 2014). We also assessed the proportion of genetic variance that could be explained by elevation in R by imputing missing genotypes with the random-forest method

MissForest (v1.4), conducting a redundancy analysis in Vegan (v2.5-7), and calculating the adjusted r^2 value and predictor p-values of the resulting model with ANOVA in Stats (v4.1.1).

Infection dynamics across elevations

We analyzed the site-level effects and apparent sublethal impacts of *Bd* in R (v4.0.2; see Supporting information for details). To ascertain whether frog population density might change substantially across elevations, influencing site-level infection dynamics, we used GLMs in MASS (v7.3-54) to examine the relationship between the elevation and counts of adults captured per site. Adult counts per site did not correlate with elevation for *P. marmoratum* (n_{sites} = 63; Fig. S2a) or *T. marmoratus* (n_{sites} = 17; Fig. S2b), so though adult counts of *R. spinulosa* declined gently with elevation (n_{sites} = 25, $p < 0.001$, Fig. S2c, Table S3), we did not include a proxy of frog density in subsequent models of site-level infection metrics. To investigate whether elevation was a good predictor of site infection metrics at *Bd*+ sites, we tested the fit of linear and quadratic regression models. The site infection metrics we used were site prevalence, which represented the proportion of infected frogs at a site; mean infection intensity, which communicated the average infection intensity of *Bd*+ frogs at a site; and site maximal infection intensity, which represented the highest pathogen load at a site. Unfortunately, we did not record signs of disease like excessive sloughing with sufficient frequency to report relationships between these symptoms and elevation.

We examined whether frog body size (SVL) and condition (SMI; as per Peig and Green 2009) responded to site infection status (*Bd*+/-), elevation, and the interaction between these terms

using GLMMs in lme4. We included site as a random effect in all models, and Gosner developmental stage as a partial correlate predicting tadpole SVLs. Though we collected data on sex for adult individuals, we excluded this variable from our analyses as it was not a significant contributor to our models. We built models for the species-life stage combinations for which we had sufficient data: *P. marmoratum* adults, *P. marmoratum* tadpoles, and *T. marmoratus* tadpoles. Published literature does not yield expectations for how body size or condition relates to elevation in these species, so we examined samples at *Bd*- sites to establish these baseline trends. To explore how thermal regimes along the elevational gradient might relate to observed trends in infection metrics and apparent sublethal impacts, we also plotted March-April temperature data from recovered iButtons relative to the temperature-dependent logistic growth rate (r) of a tropical *Bd* strain (Voyles *et al.* 2017), the CT_{max} of adult *P. marmoratum*, and the mean temperature tolerated by *P. marmoratum* adults that recovered following freezing (Reider *et al.* 2020).

RESULTS

Phylogenetic placement, spatial genetic structure, and local adaptation

Vilcanota *Bd* samples from *P. marmoratum* (n = 44) nest within the *Bd*GPL-2 clade of the *Bd*GPL lineage but do not cluster together relative to a panel of globally-derived *Bd*GPL genotypes in a consensus gene tree or PCA (Fig. 2, Fig. 3a). Vilcanota *Bd* is geographically unstructured, with samples failing to cluster geographically in a PCA (Fig. 3b), despite containing many low-frequency variants robust to stringent filtering (73.4% variants have an

allele frequency of ~1%). Watersheds or sites were not differentiated according to an AMOVA ($p > 0.05$, Table S1). Elevation was a significant predictor of genetic variance according to redundancy analysis but only explained 1.2% of genetic variance ($p < 0.05$, Table S2).

Site infection metrics across elevations

We detected *R. spinulosa* only up to 4,895 m asl. We recorded adult *Pleurodema marmoratum* and *Telmatobius marmoratus* at the highest point of Osjollo Pass, at a maximal elevation of 5,333 and 5,226 m asl respectively. Though not true of *T. marmoratus*, we were able to sample *P. marmoratus* at regular intervals across the entirety of both Osjollo and Chimboya Passes. This continuous distribution suggests that the deglaciated passes now provide new connectivity between *P. marmoratus* populations north and south of the Vilcanota.

Bd prevalence in *P. marmoratum* was 30.0% among juveniles ($n = 120$) and 24.0% among adults ($n = 317$), but not detected in tadpoles (n = 256). The best model by AIC relating elevation to prevalence was a quadratic model, where prevalence peaked at approx. 4700 m asl (Fig. S4a, Table S4). The predictors in this model were significant and explained 20% of variance in prevalence ($n_{sites} = 18$, $p < 0.05$, Table S4). Visual inspection of site infection intensity metrics against elevation suggested that these metrics declined with increasing elevation (Fig. S4b-c), but the data supported neither a linear nor a quadratic relationship in these cases ($n_{sites} = 18$).

Sublethal impacts across elevations

In *Telmatobius marmoratus* tadpoles, a full interactive model including elevation and site infection status explained 11% of variance in body condition and minimized AIC (n = 77, n_{sites} = 6, Table S5), though this model may be overfit. All predictors were significant ($p < 0.05$) except the slope of SMI against elevation at *Bd*+ sites. This model suggested that tadpoles had higher body conditions at lower elevations for *Bd*- sites but not for *Bd*+ sites (Fig. 4a). Similarly, *T. marmoratus* tadpole body size (SVL) was best predicted by a full interactive model that included elevation, site status, and developmental stage. All predictors were significant, with fixed effects explaining 68% of the variance (n = 77, n_{sites} = 6, $p < 0.001$, Table S6). Consistent with our findings regarding *T. marmoratus* tadpole SMI, this model suggested that tadpoles are longer relative to developmental stage at lower elevations but only at *Bd*- sites (Fig. 4b). The relationships between *T. marmoratus* tadpole SMI or SVL and elevation cannot be attributed to differences in phenology across elevation (Fig. S6d).

The model predicting *P. marmoratum* tadpole SMI from elevation and site status with lowest AIC included elevation only. According to this model, body condition declined with increasing elevation, but the model predictors were not significant, and the fixed effects explained only 4% of variance in SMI (n = 128, n_{sites} = 15, p >0.05, Table S5). Visual inspection of these data revealed that SMI appeared reduced for lower elevation tadpoles at *Bd*+ sites, similar to trends detected for *T. marmoratus* tadpoles (compare Fig. 4a and Fig. S5a). Indeed, a model including site status and its interaction with elevation was within a ΔAIC of only 0.02 of the elevation-only model, explained 7% of variance in SMI, and included a significant slope and intercept at *Bd*- sites (Table S5). Meanwhile, *Pleurodema marmoratum* tadpole SVL was best predicted by elevation alone. Tadpoles were longer relative to developmental stage at higher elevations

302 regardless of site infection status (Fig. S6a). The model explained 18% of variance in SVL, but
303 not all predictors were significant (n = 128, n_{sites} = 15, $p > 0.05$, Table S6). In the case of *P.*
304 *marmoratum*, differences in phenology across elevations could potentially contribute to
305 relationships between elevation and body condition (Fig. S6c); however, this phenomenon would
306 presumably impact *Bd*+ and *Bd*- sites alike.
307
308 In *P. marmoratum* adults, the best model of SMI by AIC was an additive model that included
309 elevation and site infection status, though these predictors were not significant and explained
310 only 3% of variance in SMI (n = 339, n_{sites} = 53, $p > 0.05$, Table S5). Based on this model, adults
311 had lower body conditions at high than at low elevations, and at *Bd*+ than at *Bd*- sites. Visual
312 inspection of these data reflects the trends that emerged for *T. marmoratus* tadpoles (compare
313 Fig. 4a and Fig. S5b): SMI was depressed for lower elevation tadpoles at *Bd*+ sites. However,
314 the full interactive model was not well supported by AIC-based model comparison (Table S5).
315
316 In adult *P. marmoratum*, SVL was best predicted from a full interactive model of elevation and
317 site *Bd* infection status. Fixed effects in this model explained 9% of variance in SVL, but though
318 all the predictors were significant the intercept was not (n = 339, n_{sites} = 53, $p > 0.05$, Table S6).
319 According to this model, SVL in adult *P. marmoratum* increases with elevation, regardless of
320 site infection status. However, while SVL increases rapidly at *Bd*- sites (6.5mm per 1,000m of
321 elevation), SVL increases only gradually at *Bd*+ sites (1.4 mm per 1,000m; Fig. S6b).
322
323 Temperature data from iButtons along the elevational gradient demonstrated that higher
324 elevations were characterized by lower average daily temperatures and larger fluctuations in

daily temperature (Fig. 5a). Ephemeral pond habitats, as expected, experienced less thermal variability than adjacent terrestrial habitats (Fig. 5a). It follows that, at higher elevations, *Bd* is characterized by a lower average growth rate, but frogs also experience greater exposure to their physiological tolerance limits (Fig. 5b).

DISCUSSION

Understanding how climate change and novel pathogens interact to challenge wildlife is of critical concern to conservation and public health. Although the influence of pathogen or vector range shifts on infection dynamics has been the subject of frequent study over the past decade (e.g. Jaenson and Lindgren 2011, Zamora-Vilchis et al 2012, Dudney et al 2021, Romanello et al 2021), we know little about how the climate-driven range shifts of hosts may impact infection dynamics. Here, we have shown that these climate-driven range shifts may impact the infection dynamics of pathogens relying on direct transmission, as well as in vector-borne systems. We used genetic analyses and modeled the relationship among elevation, site infection metrics, and measures of individual energetic status to understand how the range expansion of three frog species may have impacted the course of their infection with *Batrachochytrium dendrobatidis.* We learned that one of the frogs studied (*P. marmoratum*) is using mountain passes cleared by the last 150 years of deglaciation to disperse between watersheds separated by the Cordillera Vilcanota. We learned that *Bd* is resilient to, and can disperse extensively at, even the highest elevations used by amphibians. Finally, we found evidence that some site infection metrics and apparent sublethal impacts of infection correlate with elevation, suggesting that this host range shift into new, high elevation habitats has implications for infection outcomes.

Genetic evidence suggests the recent introduction and extensive dispersal of *Bd*GPL-2

Whether global *Bd* epizootics were provoked by a novel or endemic pathogen remains an open question (Rosenblum *et al.* 2013). *Bd* was often present in areas long before recorded outbreaks (e.g. de León *et al.* 2019, Basanta *et al.* 2021). Indeed, the earliest known *Bd* was swabbed from a Titicaca water frog (*Telmatobius culeus*) collected just 300km southeast of the Cordillera Vilcanota in 1863 (Burrowes and De la Riva 2017a). Scientists responsible for this and other local pre-epizootic detections propose that they represent endemic strains, and that regional *Bd*-associated declines were driven by the introduction of a novel strain in the 1990s (Becker *et al.* 2016, Burrowes and De la Riva 2017a). This novel strain is usually presumed to be the global panzootic lineage (*Bd*GPL), the lineage most frequently associated with disease outbreaks, whose lack of genetic structure even at the global scale suggests its recent, rapid expansion (Schloegel *et al.* 2012, Rosenblum *et al.* 2013, James *et al.* 2015, O'Hanlon *et al.* 2018).

Bd samples sequenced in this study belong to *Bd*GPL, consistent with previous studies genotyping South American *Bd* collected west of the Brazilian Atlantic Forest (O'Hanlon *et al.* 2018, Byrne *et al.* 2019, Russell *et al.* 2019, Alvarado-Rybak *et al.* 2021). Further, Vilcanota *Bd* was all *Bd*GPL-2, the more derived and globalized of two *Bd*GPL sub-clades (James *et al.* 2015). However, it is worth noting that *Bd*GPL can outcompete other strains during coinfections, so may have displaced potentially pre-existing endemic strains in the Vilcanota (Farrer *et al.* 2011,

370 Jenkinson *et al.* 2018). Additionally, selecting the highest intensity swabs to sequence at each
371 site could bias our data against less-virulent strains (Farrer *et al.* 2011, Byrne *et al.* 2017).
372
373 We found Vilcanota *Bd*GPL-2 to be spatially unstructured using our genetic markers, consistent
374 with most previous genetic studies of *Bd*GPL, which have found it to be spatially unstructured
375 from local to continental scales (Velo-Antón *et al.* 2012, Byrne *et al.* 2019, Alvarado-Rybak *et*
376 *al.* 2021, Basanta *et al.* 2021, Rothstein *et al.* 2021). This lack of structure has often been
377 interpreted as evidence for its recent introduction to the sampled area, though might simply
378 indicate high connectivity between amphibian populations. One exception to the general lack of
379 spatial structuring in *Bd* has been the Sierra Nevada of California, suggesting the western U.S.A.
380 as a potential origin for *Bd*GPL (Rothstein *et al.* 2021). Sierran *Bd* demonstrates both that
381 *Bd*GPL can develop spatial structure and that it can do so despite cool, high-elevation conditions
382 that may constrain rates of evolutionary change.
383
384 Though unstructured, Vilcanota *Bd* has substantial low-frequency variation, representative of the
385 global variation in *Bd*GPL-2. Our data cannot exclude the possibility that *Bd*GPL circulated in
386 the Vilcanota prior to the local epizootics of the early 2000s, but in the context of prior regional
387 studies (Lips *et al.* 2008, Catenazzi *et al.* 2011, Burrowes *et al.* 2020) it is most likely that
388 *Bd*GPL-2 housed substantial standing genetic variation upon its introduction or that it was
389 introduced multiple times. Our analyses place Vilcanota *Bd* in a large, global polytomy in
390 *Bd*GPL-2, so we cannot determine whether *Bd*GPL spread from Ecuador via the Andes (Lips *et*
391 *al.* 2008) or from Brazil via Bolivia (Catenazzi *et al.* 2011, Burrowes *et al.* 2020). However, the
392 timing of *Bd*GPL-2's arrival likely coincides with the onset of amphibian die-offs in the

Vilcanota in the early 2000s (Seimon *et al.* 2005, 2007), as this corresponds to declines in adjacent Amazonian and cloud forest regions (Catenazzi *et al.* 2011).

Regardless of the provenance and timing of introduction, our data demonstrates that *Bd*GPL-2 has undergone extensive, frequent dispersal locally. It is clear the transmission of *Bd* across the Cordillera Vilcanota was not limited to transmission by frogs along the terrestrial corridors provided by deglaciated passes. Processes facilitating its dispersal might include *the* trade of *T. marmoratus* for urban consumption (Catenazzi *et al.* 2010), the introduction and harvest of nonnative fish (Ortega and Hidalgo 2008, Martín-Torrijos *et al.* 2016), the movements of Andean waterbirds (Burrowes and De la Riva 2017b), or even precipitation (Kolby *et al.* 2015).

Amphibians cannot escape *Bd* by range shifting upslope

Early studies generally found that *Bd* infection prevalence or intensity increased with elevation (Brem and Lips 2008) and epizootics impacted highland sites more severely (Lips 1999, Berger *et al.* 2004, Lips *et al.* 2006). These relationships are consistent with the preference of *Bd* for cool temperatures (Piotrowski *et al.* 2004, Woodhams *et al.* 2008) and the impaired function of the amphibian immune system and skin microbiome at colder, more thermally variable high elevations (Jackson and Tinsley 2002, Daskin *et al.* 2014). Early field studies did not sample above 2,500 m asl, but empirical work demonstrating that suboptimal temperatures retard *Bd* growth led to a hypothesis that *Bd* pathogenicity was restricted to below 4,000 m asl (Piotrowski *et al.* 2004, Ron 2005, Pounds *et al.* 2006, Woodhams *et al.* 2008). Subsequent studies of *Bd* dynamics up to 4,000 m asl reported declining infection prevalence or intensity with increasing

elevation (Muths *et al.* 2008, Catenazzi *et al.* 2011), perhaps due as much to increasing aridity as to decreasing temperatures at these higher elevations (De la Riva and Burrowes 2011).

The idea that *Bd* pathogenicity had an upper elevational bound was later undermined by severe infections documented above 4,000 m asl in the Vilcanota and other sites (Seimon *et al.* 2005, 2007, Knapp *et al.* 2011). Here, we find limited evidence that elevational extremes constrain *Bd* growth. *Bd* infection metrics appear to decline at the upper reaches of the elevational gradient colonized by Vilcanota frogs (3,967—5,333 m asl)—both for the significant and well-fit quadratic model of prevalence and for the inherently noisy infection intensity data. Such declines would be consistent with our expectations following from temperature data recorded by our iButtons, considered in light of a study profiling the thermal dependence of *Bd* growth (Voyles *et al.* 2017): *Bd* likely experience lower growth rates at higher elevations in the Vilcanota (Fig. 5).

Upslope range shifts may mediate infection outcomes through exposure to thermal variability

We investigated whether extreme elevations compounded or ameliorated the apparent sublethal impacts of *Bd* by comparing frog body size and condition at *Bd*+ and *Bd*- sites. Body size and condition signal important information about nutritional history in amphibian larvae, juveniles, and adults; and can predict important fitness components such as fecundity, the ability to respond effectively to environmental stress, and lifespan (Metcalfe and Monaghan 2001, Hector *et al.* 2012, MacCracken and Stebbings 2012, Martins *et al.* 2013, Brodeur *et al.* 2020). To call sites as *Bd*- we required infection intensities for at least 10 postmetamorphic frogs at that site, with

439 individual frog infection statuses being called from triplicate qPCR reactions; therefore, though
440 we lacked longitudinal sampling that would more definitely classify our sites as *Bd*- or *Bd*+, we
441 believe our protocol minimizes the risk of both false negatives and false positives.
442
443 At *Bd*- sites, *Telmatobius marmoratus* tadpole condition and size declined with increasing
444 elevations, which our examination of adult counts across elevations suggests we cannot attribute
445 to increased competition. *T. marmoratus* tadpoles have a protracted larval development relative
446 to *P. marmoratum* and *R. spinulosa*. During the estimated 5—19 months until metamorphosis
447 (Rodríguez-Papuico 1974, PNUD and ALT 2002, Lobos *et al.* 2018), they rely upon the
448 resources of their natal stream (Catenazzi *et al.* 2013a, Rubio 2019). Therefore, declines in
449 stream primary productivity with increasing elevation (Jacobsen 2008) might explain this trend
450 in tadpoles. An alternative explanation could be that *T. marmoratus* tadpoles metamorphose
451 more quickly at higher elevations, attaining a smaller size in the process (Licht 1975).
452
453 For larval *T. marmoratus*, circulating *Bd* was associated with lower body condition and size
454 relative to developmental stage, but only at low elevations. This interaction is consistent with
455 expectations from our temperature data. Aquatic microhabitats at extreme elevations are
456 frequently at no- or low-growth temperatures for *Bd*, resulting in a depressed average growth
457 rate, but at low elevation remain stably at temperatures conducive to *Bd* growth (Fig. 5, Fig. S7).
458 Studies of other amphibian species have shown that *Bd* infection can result in smaller or lighter
459 tadpoles (Parris and Cornelius 2004, Catenazzi *et al.* 2013b). Infected tadpoles may sacrifice
460 body size and condition by diverting energy towards immune response or by accelerating
461 metamorphosis (Warne *et al.* 2011). However, we expect that, for slow-developing *T.*

462 *marmoratus*, the impact of *Bd* on tadpole mouthparts is particularly important: *Bd* infects
463 keratinized tissues, which in tadpoles limits *Bd* growth to their mouthparts and causes oral
464 deformities over time (Berger *et al.* 1998, Vredenburg and Summers 2001), as has been
465 demonstrated for congenerics (Rubio 2019). Damaged mouthparts can reduce tadpole feeding
466 efficiency, reshape their feeding ecology, and retard their growth (Rowe *et al.* 1996, Rachowicz
467 and Vredenburg 2004, Rubio 2019).
468
469 Shared mechanisms may contribute to a similar trend in larval *P. marmoratum* body condition.
470 Their body condition declines with increasing elevations at *Bd*- sites, but *Bd* infections appear to
471 take a larger energetic toll on *P. marmoratum* tadpoles at lower elevations. Unlike larval *T.*
472 *marmoratus*, larval *P. marmoratum* increase in body size relative to developmental stage with
473 elevation regardless of site infection status. This trend may reflect a reproductive strategy that is
474 advantageous under stressful, high elevation conditions: females produce fewer offspring of
475 higher quality in harsher environments. This strategy has been documented in several frog
476 species (e.g., Lüddecke 2002, Räsänen *et al.* 2005, Liao *et al.* 2014). Given the decline in
477 abundance and eventual disappearance of *R. spinulosa* with increasing elevations, it is
478 conceivable that this trend instead results from decreasing competition for food from other
479 tadpoles, as *P. marmoratum* and *R. spinulosa* sometimes share larval habitat at lower elevations.
480
481 Adult *P. marmoratum* body size also increases with elevation, perhaps owing to either reduced
482 competition with *R. spinulosa* or selection for larger size at metamorphosis and larger females
483 capable of greater maternal investment (Chen *et al.* 2013, Liao *et al.* 2014, Womack and Bell
484 2020). However, their body size increases dramatically with elevation at *Bd*- sites, while only

485 gradually at *Bd*+ sites (6.5mm vs. 1.4mm per 1,000m of elevation). In this case, *Bd* appears to
486 have a larger sublethal toll at higher elevations. While terrestrial animals experience lower
487 average *Bd* growth rates at extreme elevations, as animals inhabiting aquatic microhabitats, they
488 are not as thermally buffered from harsh temperature extremes. We found that adult *P.*
489 *marmoratum* are more exposed to their thermal tolerance limits at extreme high elevations (Fig.
490 5, Fig. S7), placing them at a fitness disadvantage relative to the *Bd* pathogen (Cohen *et al.* 2017,
491 2019). Their failure to respond phenotypically to high-elevation conditions could compromise
492 their fecundity and survivorship, suggesting that extreme elevations may compound rather than
493 ameliorate the stress of *Bd* infection for *P. marmoratum* adults.
494
495 It is important to note that all association between *Bd* site status and apparent sublethal impacts
496 to individuals are correlative in this study. We did not conduct trials and cannot know the *Bd*
497 exposure history of any individual frog. One important implication is that we do not know the
498 direction of causality. Although here we have interpreted that *Bd* could be incurring sublethal
499 impacts, an alternate explanation for any associations we have observed is that *Bd* is more likely
500 to affect amphibian populations with lower energy reserves. If this were the case, observed
501 interactions between body condition or size, elevation, and site *Bd* status require different
502 mechanistic explanations.
503

504 # CONCLUSION

505
506 Climate change will continue to drive range shifts, with many species expanding into more
507 thermally-variable regions like the Vilcanota. It is important that we understand how the stress of

508 novel, frequently less optimal, habitats impact host-pathogen systems, particularly in the face of
509 increasingly common emerging infectious disease challenges. In the case of amphibian-*Bd*
510 systems, hosts cannot escape this pathogen by range shifting upslope. *Bd* can infect amphibians
511 even at the edges of their physiological tolerances, though factors like exposure to thermal
512 variability may mediate infection outcomes. *Bd* has apparently undergone frequent dispersal
513 across the extreme elevation habitat of the Cordillera Vilcanota, with transmission around this
514 barrier not dependent on the formation of deglaciated dispersal corridors. This work can help
515 inform and stimulate further questions around how host range shifts might in some cases
516 exacerbate and in others mitigate emerging infectious disease events.
517

518 # REFERENCES

519
520 Alvarado-Rybak *et al.* 2021. Chytridiomycosis outbreak in a Chilean giant frog (*Calyptocephalella gayi*)
521 captive breeding program: Genomic characterization and pathological findings. – Front. Vet. Sci. 8:
522 1–9.
523 Basanta, M. D. *et al.* 2021. Early presence of *Batrachochytrium dendrobatidis* in Mexico with a
524 contemporary dominance of the global panzootic lineage. – Mol. Ecol. 30: 424–437.
525 Becker, C. G. *et al.* 2016. Historical dynamics of *Batrachochytrium dendrobatidis* in Amazonia. –
526 Ecography. 39: 954–960.
527 Berger, L. *et al.* 1998. Chytridiomycosis causes amphibian mortality associated with population declines
528 in the rain forests of Australia and Central America. – Proc. Natl. Acad. Sci. 95: 9031–9036.
529 Berger, L. *et al.* 2004. Effect of season and temperature on mortality in amphibians due to
530 chytridiomycosis. – Aust. Vet. J. 82: 31–36.
531 Bosch, J. *et al.* 2007. Climate change and outbreaks of amphibian chytridiomycosis in a montane area of

Central Spain; is there a link? – Proc. R. Soc. B Biol. Sci. 274: 253–260.

Boyle, A.H.D. *et al.* 2007. Diagnostic assays and sampling protocols for the detection of *Batrachochytrium dendrobatidis*. – Dis. Aquat. Organ. 73: 175–192.

Brem, F. M. R. and Lips, K. R. 2008. *Batrachochytrium dendrobatidis* infection patterns among Panamanian amphibian species, habitats and elevations during epizootic and enzootic stages. – Dis. Aquat. Organ. 81: 189–202.

Brodeur, J. C. *et al.* 2020. Frog body condition: Basic assumptions, comparison of methods and characterization of natural variability with field data from *Leptodactylus latrans*. – Ecol. Indic. 112: 106098.

Burrowes, P. A. and De la Riva, I. 2017a. Unraveling the historical prevalence of the invasive chytrid fungus in the Bolivian Andes: implications in recent amphibian declines. – Biol. Invasions 19: 1781–1794.

Burrowes, P. and De la Riva, I. 2017b. Detection of the amphibian chytrid fungus *Batrachochytrium dendrobatidis* in museum specimens of Andean aquatic birds: Implications for pathogen dispersal. – J. Wildl. Dis. 53: 349–355.

Burrowes, P. A. *et al.* 2004. Potential causes for amphibian declines in Puerto Rico. – Herpetologica 60: 141–154.

Burrowes, P. A. *et al.* 2020. Genetic analysis of post-epizootic amphibian chytrid strains in Bolivia: Adding a piece to the puzzle. – Transbound. Emerg. Dis. 67: 2163–2171.

Bustamante, M. R. *et al.* 2005. Cambios en la diversidad en siete comunidades de anuros en los Andes de Ecuador. – Biotropica 37: 180–189.

Byrne, A. Q. *et al.* 2017. Unlocking the story in the swab: A new genotyping assay for the amphibian chytrid fungus *Batrachochytrium dendrobatidis*. – Mol. Ecol. Resour. 17: 3218–3221.

Byrne, A. Q. *et al.* 2019. Cryptic diversity of a widespread global pathogen reveals expanded threats to amphibian conservation. – Proc. Natl. Acad. Sci. 116: 20382–20387.

Catenazzi, A. *et al.* 2010. *Batrachochytrium dendrobatidis* in the live frog trade of Telmatobius (Anura :

558 Ceratophryidae) in the tropical Andes. – Dis. Aquat. Organ. 92: 187–191.
559 Catenazzi, A. *et al.* 2011. *Batrachochytrium dendrobatidis* and the collapse of anuran species richness
560 and abundance in the Upper Manu National Park, Southeastern Peru. – Conserv. Biol. 25: 382–391.
561 Catenazzi, A. *et al.* 2013a. Conservation of the high Andean frog *Telmatobius jelskii* along the PERU
562 LNG pipeline in the Regions of Ayacucho and Huancavelica, Peru. – In: Alonso, A. *et al.* (eds),
563 Monitoring biodiversity: Lessons from a Trans-Andean megaproject. Smithsonian Scholarly Press,
564 Washington, DC.
565 Catenazzi, A. *et al.* 2013b. High prevalence of infection in tadpoles increases vulnerability to fungal
566 pathogen in high-Andean amphibians. – Biol. Conserv. 159: 413–421.
567 Catenazzi, A. *et al.* 2017. Epizootic to enzootic transition of a fungal disease in tropical Andean frogs :
568 Are surviving species still susceptible? – PloS One 12: e0186478.
569 Chen, W. *et al.* 2013. Maternal investment increases with altitude in a frog on the Tibetan Plateau. – J.
570 Evol. Biol. 26: 2710–2715.
571 Cohen, J. M. *et al.* 2017. The thermal mismatch hypothesis explains host susceptibility to an emerging
572 infectious disease. – Ecol. Lett. 20: 184–193.
573 Cohen, J. M. *et al.* 2019. An interaction between climate change and infectious disease drove widespread
574 amphibian declines. – Glob. Chang. Biol. 25: 927-937.
575 Daskin, J. H. *et al.* 2014. Cool temperatures reduce antifungal activity of symbiotic bacteria of threatened
576 amphibians – Implications for disease management and patterns of decline. – PloS One 9: e100378.
577 De la Riva, I. and Burrowes, P. A. 2011. Rapid assessment of the presence of *Batrachochytrium*
578 *dendrobatidis* in bolivian Andean frogs. – Herpetol. Rev. 42: 372–375.
579 De León, M. E. *et al.* 2019. *Batrachochytrium dendrobatidis* infection in amphibians predates first known
580 epizootic in Costa Rica. – PloS One 14: 1–14.
581 Dudney, J. *et al.* 2021. Nonlinear shifts in infectious rust disease due to climate change. – Nat. Commun.
582 12: 1—13.
583 Edgar, R. C. 2004. MUSCLE: Multiple sequence alignment with high accuracy and high throughput. -

584 Nucleic Acids Res. 32: 1792–1797.
585 Enriquez-Urzelai, U. *et al.* 2019. Are amphibians tracking their climatic niches in response to climate
586 warming? A test with Iberian amphibians. - Clim. Change 154: 289–301.
587 Farrer, R. A. *et al.* 2011. Multiple emergences of genetically diverse amphibian infecting chytrids include
588 a globalized hypervirulent recombinant lineage. - PNAS 108: 1–6.
589 Fisher, M. C. *et al.* 2012. Emerging fungal threats to animal, plant and ecosystem health. - Nature 484: 1–
590 18.
591 Freeman, B. G. *et al.* 2018. Climate change causes upslope shifts and mountaintop extirpations in a
592 tropical bird community. - Proc. Natl. Acad. Sci. 115: 11982–11987.
593 Gosner, K. L. . 1960. A simplified table for staging anuran embryos and larvae with notes on
594 identification. - Herpetologica 16: 183–190.
595 Haddad, N. M. *et al.* 2014. Potential negative ecological effects of corridors. - Conserv. Biol. 28: 1178–
596 1187.
597 Harvell, C. D. *et al.* 2002. Climate warming and disease risks for terrestrial and marine biota. - Science
598 (80-.). 296: 2158–2162.
599 Hector, K. L. *et al.* 2012. Consequences of compensatory growth in an amphibian. - J. Zool. 286: 93–101.
600 Hoberg, E. P. and Brooks, D. R. 2015. Evolution in action: climate change, biodiversity dynamics and
601 emerging infectious disease. - Philos. Trans. R. Soc. B-Biological Sci. 370: 7.
602 Jackson, J. and Tinsley, R. 2002. Effects of environmental temperature on the susceptibility of *Xenopus*
603 *laevis* and *X. wittei* (Anura) to *Protopolystoma xenopodis* (Monogenea). - Parasitol. Res. 88: 632–
604 638.
605 Jacobsen, D. 2008. Tropical high-altitude streams. - In: Tropical Stream Ecology. Academic Press, pp.
606 219–256.
607 Jaenson, T.G. and Lindgren, E. 2011. The range of *Ixodes ricinus* and the risk of contracting Lyme
608 borreliosis will increase northwards when the vegetation period becomes longer. Ticks and tick-
609 borne diseases 2: 44—49.

610 James, T. Y. *et al.* 2015. Disentangling host, pathogen, and environmental determinants of a recently
611 emerged wildlife disease: Lessons from the first 15 years of amphibian chytridiomycosis research. -
612 Ecol. Evol. 5: 4079–4097.
613 Jenkinson, T. S. *et al.* 2018. Globally invasive genotypes of the amphibian chytrid outcompete an
614 enzootic lineage in coinfections. - Proc. B 285: 20181894.
615 Jones, K. E. *et al.* 2008. Global trends in emerging infectious diseases. - Nature 451: 990–993.
616 Kamvar, Z. *et al.* 2014. Poppr: an R package for genetic analysis of populations with clonal, partially
617 clonal, and/or sexual reproduction. - PeerJ 2: e281.
618 Knapp, R. A. *et al.* 2011. Nowhere to hide: impact of a temperature-sensitive amphibian pathogen along
619 an elevation gradient in the temperate zone. - Ecosphere 2: 1–26.
620 Kolby, J. E. *et al.* 2015. Presence of amphibian chytrid fungus (*Batrachochytrium dendrobatidis*) in
621 rainwater suggests aerial dispersal is possible. - Aerobiologia 31: 411–419.
622 Korneliussen, T. S. *et al.* 2014. Open Access ANGSD : Analysis of Next Generation Sequencing Data. -
623 BMCBioinformatics 15: 356.
624 Lampo, M. *et al.* 2006. A chytridiomycosis epidemic and a severe dry season precede the disappearance
625 of Atelopus species from the Venezuelan Andes. - Herpetol. J. 16: 395–402.
626 Li, Y. *et al.* 2013. Review and synthesis of the effects of climate change on amphibians. - Integr. Zool. 8:
627 145–161.
628 Liang, L. and Gong, P. 2017. Climate change and human infectious diseases: A synthesis of research
629 findings from global and spatio-temporal perspectives. - Environ. Int. 103: 99–108.
630 Liao, W. B. *et al.* 2014. Altitudinal variation in maternal investment and trade-offs between egg size and
631 clutch size in the Andrew's toad. - J. Zool. 293: 84–91.
632 Licht, E. 1975. Comparative life history features of the western spotted frog, *Rana pretiosa*, from low-
633 and high-elevation populations. - Can. J. Zool. 53: 1254–1257.
634 Lips, K. R. 1999. Mass mortality and population declines of anurans at an upland site in Western Panama.
635 - Conserv. Biol. 13: 117–125.

636 Lips, K. R. *et al.* 2006. Emerging infectious disease and the loss of biodiversity in a Neotropical
637 amphibian community. - Proc. Natl. Acad. Sci. 103: 3165–3170.
638 Lips, K. R. *et al.* 2008. Riding the wave: Reconciling the roles of disease and climate change in
639 amphibian declines. - PLoS Biol. 6: 441–454.
640 Lobos, G. *et al.* 2018. Temporal gap between knowledge and conservation needs in high Andean
641 anurans : The case of the Ascotán salt flat frog in Chile. - South Am. J. Herpetol. 13: 33–43.
642 Lüddecke, H. 2002. Variation and trade-off in reproductive output of the Andean frog *Hyla labialis*. -
643 Oecologia 130: 403–410.
644 MacCracken, J.G., Stebbings, J.L. 2012. Test of a Body Condition Index with Amphibians. - J. Herpetol.
645 46: 346–350.
646 Martín-Torrijos, L. *et al.* 2016. Rainbow trout (*Oncorhynchus mykiss*) threaten Andean amphibians. -
647 Neotrop. Biodivers. 2: 26–36.
648 Martins, F. M. S. *et al.* 2013. Differential effects of dietary protein on early life-history and
649 morphological traits in natterjack toad (*Epidalea calamita*) tadpoles reared in captivity. - Zoo Biol.
650 32: 457–462.
651 Metcalfe, N. B. and Monaghan, P. 2001. Compensation for a bad start: Grow now, pay later? - Trends
652 Ecol. Evol. 16: 254–260.
653 Moritz, C. *et al.* 2008. Impact of a century of climate change on small-mammal communities in Yosemite
654 National Park, USA. - Science (80-.). 322: 261–264.
655 Muths, E. *et al.* 2008. Distribution and environmental limitations of an amphibian pathogen in the Rocky
656 Mountains, USA. - Biol. Conserv. 141: 1484–1492.
657 O'Hanlon, S. J. *et al.* 2018. Recent Asian origin of chytrid fungi causing global amphibian declines. -
658 Science (80-.). 360: 621–627.
659 Ortega, H. and Hidalgo, M. 2008. Freshwater fishes and aquatic habitats in Peru: Current knowledge and
660 conservation. - Aquat. Ecosyst. Heal. Manag. 11: 257–271.
661 Parmesan, C. *et al.* 1999. Poleward shifts in geographical ranges of butterfly species associated with

662 regional warming. - Nature 399: 579–583.
663 Parris, M. J. and Cornelius, T. O. 2004. Fungal pathogen causes competititve and developmental stress in
664 larval amphibian communities. - Ecology 85: 3385–3395.
665 Peig, J. and Green, A. J. 2009. New perspectives for estimating body condition from mass/length data:
666 The scaled mass index as an alternative method. - Oikos 118: 1883–1891.
667 Piotrowski, J. S. *et al.* 2004. Physiology of *Batrachochytrium dendrobatidis*, a Chytrid pathogen of
668 amphibians. - Mycologia 96: 9–15.
669 PNUD and ALT 2002. Evaluación de la población de la rana gigante del lago Titicaca *Telmatobius*
670 *culeus*. Crianza y manejo productivo de la rana gigante del lago Titicaca.
671 Poremba, R. J. *et al.* 2015. Meteorological Characteristics of Heavy Snowfall in the Cordillera Vilcanota ,
672 Peru. - 72nd East. Snow Conf.: 167–180.
673 Pounds, A. J. *et al.* 2006. Widespread amphibian extinctions from epidemic disease driven by global
674 warming. - Nature 439: 161–167.
675 Rachowicz, L. J. and Vredenburg, V. T. 2004. Transmission of *Batrachochytrium dendrobatidis* within
676 and between amphibian life stages. - Dis. Aquat. Organ. 61: 75–83.
677 Raffel, T. R. *et al.* 2013. Disease and thermal acclimation in a more variable and unpredictable climate. -
678 Nat. Clim. Chang. 3: 146–151.
679 Räsänen, K. *et al.* 2005. Maternal investment in egg size: Environment- and population-specific effects on
680 offspring performance. - Oecologia 142: 546–553.
681 Raxworthy, C. J. *et al.* 2008. Extinction vulnerability of tropical montane endemism from warming and
682 upslope displacement: A preliminary appraisal for the highest massif in Madagascar. - Glob. Chang.
683 Biol. 14: 1703–1720.
684 Reider, K. E. 2018. Survival at the summits : Amphibian responses to thermal extremes, disease, and
685 rapid climate change in the high tropical Andes by. – PhD thesis, Florida International University,
686 USA.
687 Reider, K. E. *et al.* 2020. Thermal adaptations to extreme freeze–thaw cycles in the high tropical Andes. -

Biotropica 53: 296–306.

Rodríguez-Papuico, H. 1974. Experimentos sobre adaptación, crianza y procesamiento de la rana de Junín. –PhD thesis, Universidad Nacional Agradia La Molina, Peru.

Rohr, J. R. and Raffel, T. R. 2010. Linking global climate and temperature variability to widespread amphibian declines putatively caused by disease. - Proc. Natl. Acad. Sci. 107: 8269–8274.

Romanello, M. *et al.* 2021. The 2021 report of the Lancet Countdown on health and climate change: code red for a healthy future. The Lancet 398: 1619—1662.

Ron, S. R. 2005. Predicting the distribution of the amphibian pathogen *Batrachochytrium dendrobatidis* in the new world. - Biotropica 37: 209–221.

Rosenblum, E. B. *et al.* 2013. Complex history of the amphibian-killing chytrid fungus revealed with genome resequencing data. - Proc. Natl. Acad. Sci. 110: 9385–9390.

Rothstein, A. P. *et al.* 2021. Divergent regional evolutionary histories of a devastating global amphibian pathogen. - Proceeding 288: 20210782.

Rowe, C. L. *et al.* 1996. Oral deformities in tadpoles (*Rana catesbeiana*) associated with coal ash deposition: effects on grazing ability and growth. - Freshw. Biol. 36: 727–730.

Rubio, A. O. 2019. Effects of the fungal pathogen *Batrachochytrium dendrobatidis* on the trophic ecology of tadpoles of Andean water frogs. - MS thesis, Southern Illinois University Carbondale, USA.

Russell, I. D. *et al.* 2019. Widespread chytrid infection across frogs in the Peruvian Amazon suggests critical role for low elevation in pathogen spread and persistence. - PLoS One 14: e0222718.

Scheele, B. C. *et al.* 2019. Amphibian fungal panzootic causes catastrophic and ongoing loss of biodiversity. - Science (80-.). 1463: 1459–1463.

Schloegel, L. M. *et al.* 2012. Novel, panzootic and hybrid genotypes of amphibian chytridiomycosis associated with the bullfrog trade. - Mol. Ecol. 21: 5162–5177.

Schmidt, S. K. *et al.* 2009. Microbial activity and diversity during extreme freeze – thaw cycles in periglacial soils, 5400 m elevation, Cordillera Vilcanota, Peru. - Extremophiles 13: 807–816.

714 Seimon, T. A. *et al.* 2005. Identification of chytridiomycosis in *Telmatobius marmoratus* at 4450 m in the
715 Cordillera Vilcanota of southern Peru. - Monogr. Herpetol. 7: 275–283.
716 Seimon, T. A. *et al.* 2007. Upward range extension of Andean anurans and chytridiomycosis to extreme
717 elevations in response to tropical deglaciation. - Glob. Chang. Biol. 13: 288–299.
718 Seimon, T. A. *et al.* 2017. Long-term monitoring of tropical alpine habitat change, Andean anurans, and
719 chytrid fungus in the Cordillera Vilcanota, Peru: Results from a decade of study. - Ecol. Evol. 7:
720 1527–1540.
721 Skerratt, L. F. *et al.* 2007. Spread of chytridiomycosis has caused the rapid global decline and extinction
722 of frogs. - Ecohealth 4: 125–134.
723 Velo-Antón, G. *et al.* 2012. Amphibian-killing fungus loses genetic diversity as it spreads across the New
724 World. - Biol. Conserv. 146: 213–218.
725 Voyles, J. *et al.* 2017. Diversity in growth patterns among strains of the lethal fungal pathogen
726 *Batrachochytrium dendrobatidis* across extended thermal optima. - Oecologia 184: 363–373.
727 Vredenburg, V. T. and Summers, A. P. 2001. Field identification of chytridiomycosis in *Rana muscosa*
728 (Camp 1915). - Herpetol. Rev. 32: 151–152.
729 Wang, Q.-W. *et al.* 2014. Is UV-induced DNA damage greater at higher elevation? - Am. J. Bot. 101:
730 796–802.
731 Warne, R. W. *et al.* 2011. Escape from the pond: Stress and developmental responses to ranavirus
732 infection in wood frog tadpoles. - Funct. Ecol. 25: 139–146.
733 Womack, M. C. and Bell, R. C. 2020. Two-hundred million years of anuran body-size evolution in
734 relation to geography, ecology and life history. - J. Evol. Biol. 33: 1417–1432.
735 Woodhams, D. C. *et al.* 2008. Life-history trade-offs influence disease in changing climates: Strategies of
736 an amphibian pathogen. - Ecology 89: 1627–1639.Zamora-Vilchis, I. *et al.* 2012. Environmental
737 temperature affects prevalence of blood parasites of birds in an elevation gradient: implications for
738 disease in a warming climate. - PloS one 7: p.e39208.
739

740

741 # FIGURES

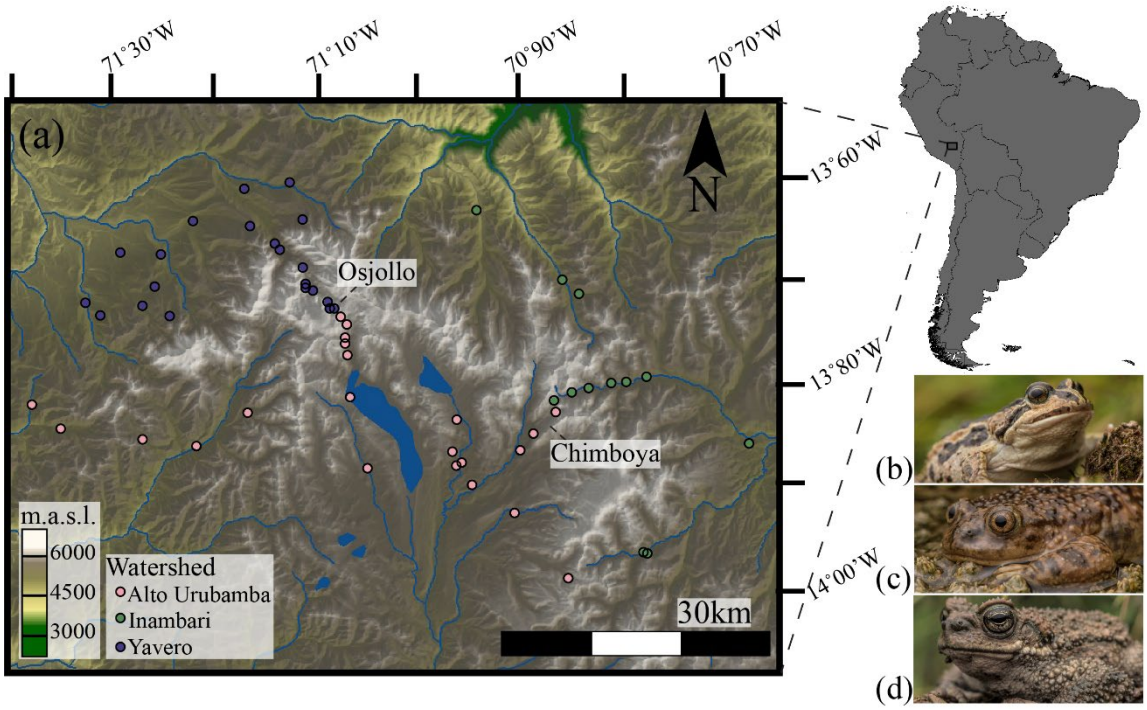

Figure 1. The study system. **(a)** Sites where amphibians and *Batrachochytrium dendrobatidis* were sampled in the Cordillera Vilcanota, colored to represent their watershed location and plotted over a hillshaded digital elevation model (DEM). The two deglaciated mountain passes, Osjollo and Chimboya, are labeled. The study species **(b)** *Pleurodema marmoratum*, **(c)** *Telmatobius marmoratus*, and **(d)** *Rhinella spinulosa* are also pictured. Photos courtesy of Anton Sorokin.

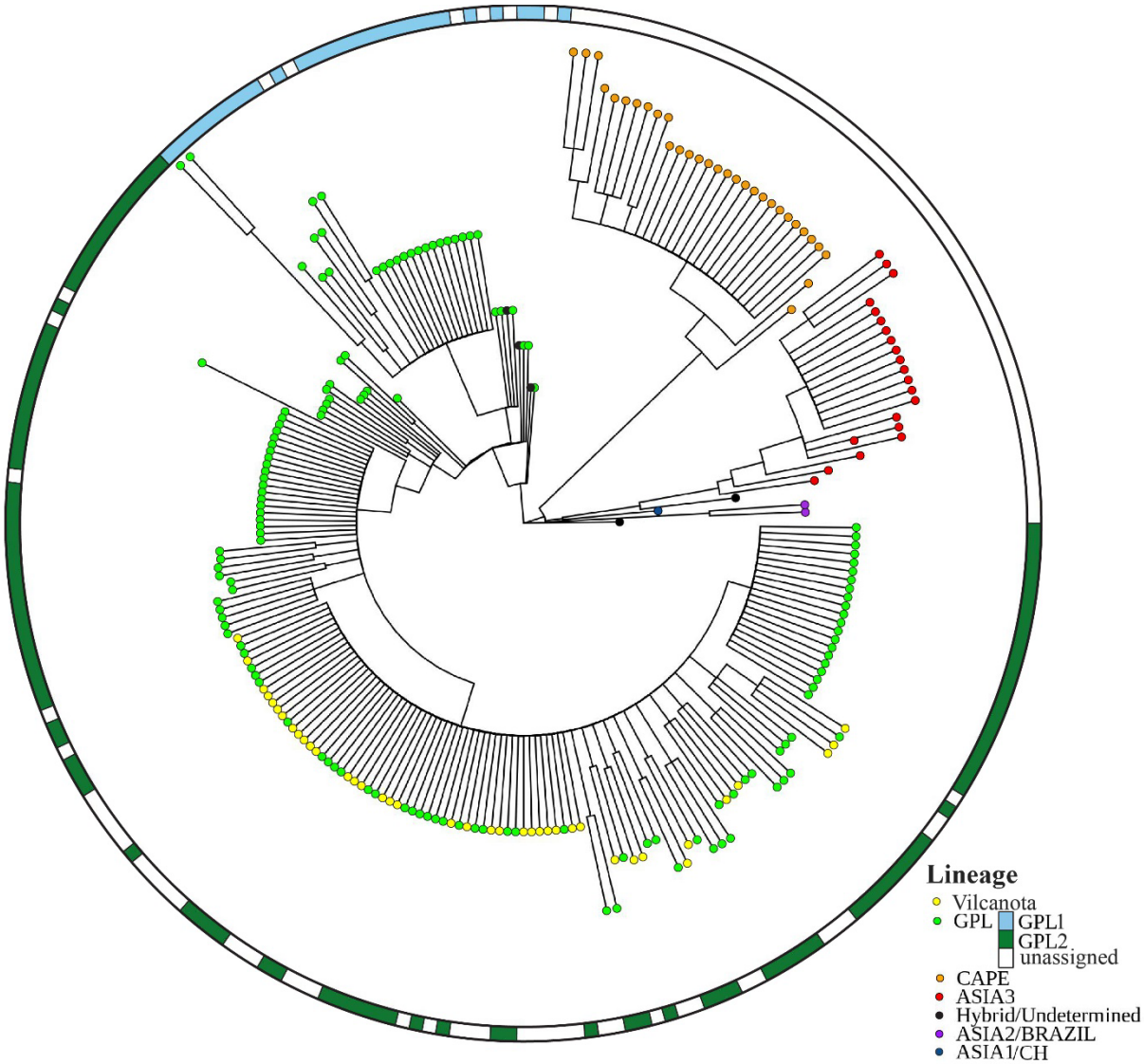

Figure 2. A midpoint-rooted consensus gene tree of Vilcanota *Bd* sampled from *Pleurodema marmoratum* (yellow tips) alongside previously-published samples representative of the five major *Bd* lineages (CAPE, ASIA3, ASIA2/BRAZIL, ASIA1/CH, GPL) and their hybrids (Byrne *et al.* 2019). This tree has a normalized quartet score of 0.807 and includes only nodes with a posterior probability ≥0.7. Assignment of *Bd*GPL samples to *Bd*GPL-1 or *Bd*GPL-2 is included whenever assigned by previous studies *(Schloegel et al. 2012, James et al. 2015, Rothstein et al.* 2021) and is shown in the concentric mosaic. This tree is included with sample names and the continent of swab origin in the supplements (Fig. S1).

748

749

750

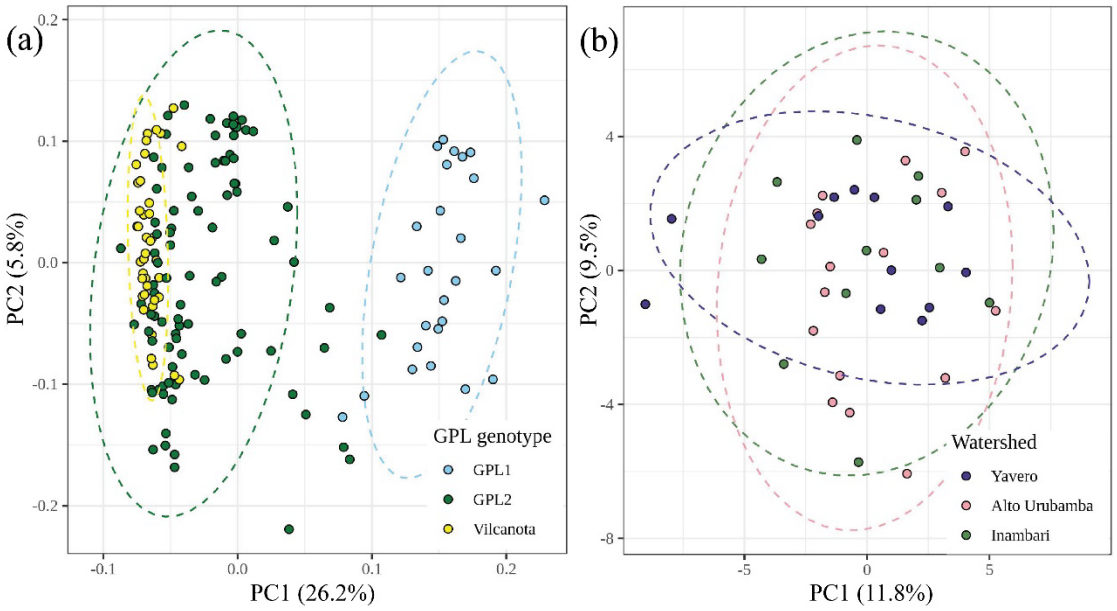

751

Figure 3. Principal component analyses (PCAs) of **(a)** global *Bd*GPL samples, demonstrating how *Bd* sampled from *Pleurodema marmoratum* in the Vilcanota is nested within the *Bd*GPL-2, and **(b)** Vilcanota samples, colored by watershed, showing their lack of spatial genetic structure.

752

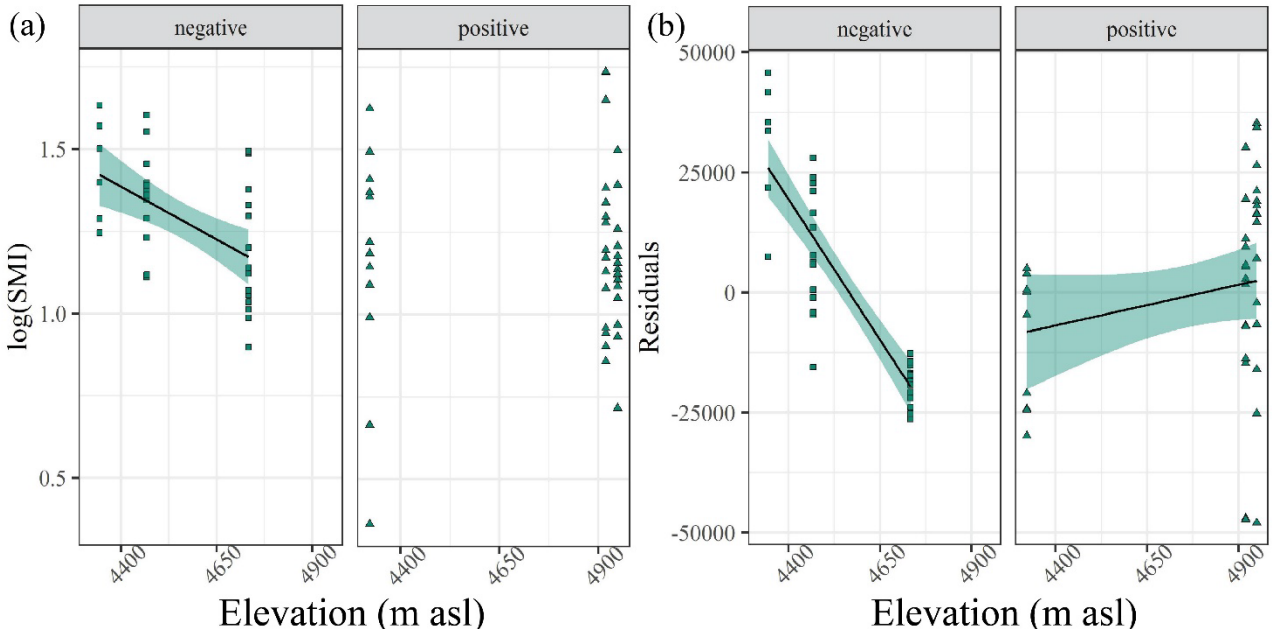

Figure 4. The relationship between elevation, site *Bd* infection status, and energetic status for *T. marmoratus* tadpoles. **(a)** Results of linear mixed model of *T. marmoratus* tadpole body condition (SMI) along the elevational gradient, displayed in separate panels for *Bd*-positive and *Bd*-negative sites as site infection status was a significant contributor to these models. **(b)** Results of linear mixed model of *T. marmoratus* tadpole residuals of body size (SVL) against Gosner stage, displayed in separate panels for *Bd*-positive and *Bd*-negative sites as site infection status was a significant contributor to these models. These trends do not appear to be attributable to differences in phenology across elevations (Fig S 6d).

753

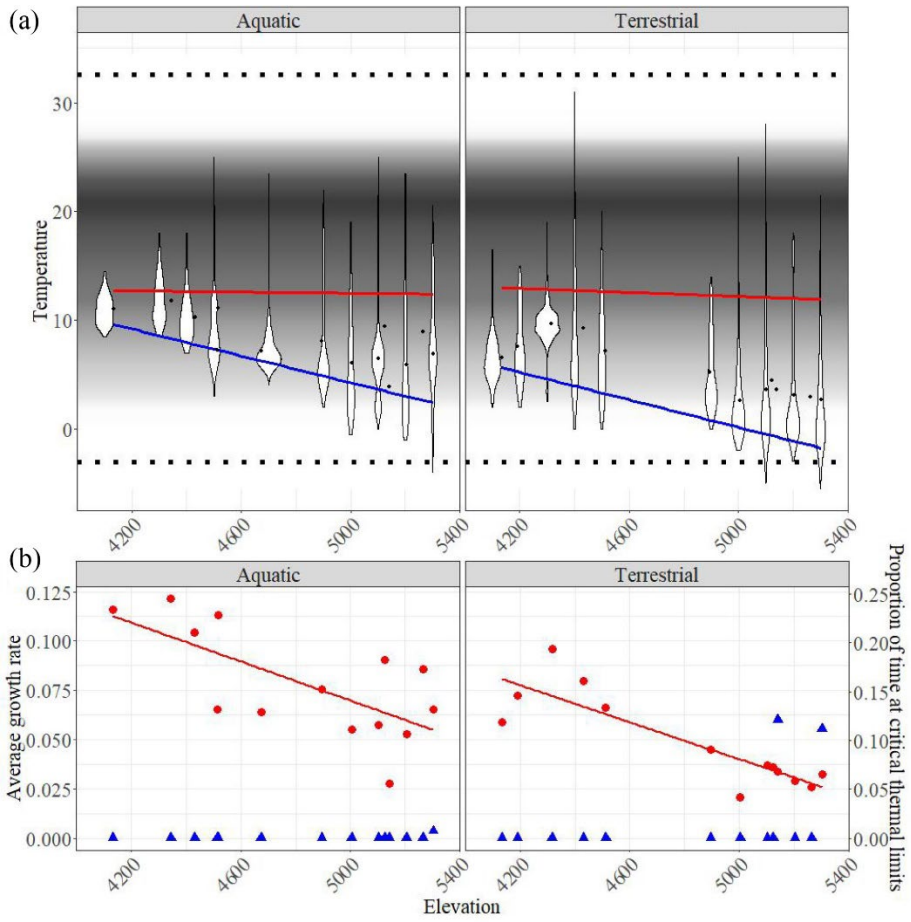

754

755 **Figure 5.** Thermal regimes along the elevational gradient and across microhabitats. **(a)** Violin plots of
756 raw temperature data. Mean daily temperatures measured by a given iButton are displayed as black
757 points. The red and blue lines represent linear regression of maximal and minimal daily temperatures,
758 respectively. The greyscale gradient represents the logistic growth rate (r) of a tropical *Bd* strain
759 quantified across temperatures by Voyles *et al.* 2017. The upper black dotted line represents the CT_{max} of
760 adult *P. marmoratum* (32.56˚C), and the lower dotted line represents the mean temperature tolerated by *P.*
761 *marmoratum* adults that recovered following freezing (Reider et al 2020). **(b)** Red points represent the
762 average growth rate of *Bd* according to the temperatures recorded by a given iButton, and the red line
763 represents a linear regression of this data. Blue triangles represent the proportion of time a given iButton
764 was exposed to temperatures outside the physiological tolerance of *P. marmoratum* adults.